Metabolic Mapping of MCF10A Human Breast Cells via Multiphoton Fluorescence Lifetime Imaging of the Coenzyme NADH

Damian K. Bird,[1] Long Yan,[1,2] Kristin M. Vrotsos,[2] Kevin W. Eliceiri,[1] Emily M. Vaughan,[3] Patricia J. Keely,[3] John G. White,[1] and Nirmala Ramanujam[2]

[1]Laboratory for Optical and Computational Instrumentation, Departments of [2]Biomedical Engineering and [3]Pharmacology, University of Wisconsin-Madison, Madison, Wisconsin

Abstract

Biochemical estimation of NADH concentration is a useful method for monitoring cellular metabolism, because the NADH/NAD$^+$ reduction-oxidation pair is crucial for electron transfer in the mitochondrial electron chain. In this article, we present a novel method for deriving functional maps of intracellular reduction-oxidation ratio *in vivo* via measurement of the fluorescence lifetimes and the ratio of free and protein-bound NADH using two-photon fluorescence lifetime imaging (FLIM). Through systematic analysis of FLIM data from the control cells, it was observed that there is a statistically significant decrease in the fluorescence lifetime of both free and protein-bound NADH and the contribution of protein-bound NADH as cells progress from an early to logarithmic to confluent phase. Potassium cyanide (KCN) treatment and serum starvation of cells yielded similar changes. There was a statistically significant decrease in the fluorescence lifetime of protein-bound and free NADH at the early and logarithmic phase of the growth curve and a statistically significant decrease in the contribution of protein-bound NADH relative to that observed in the control cells at all three phases of the growth curve. The imposed perturbations (confluence, serum starvation, and KCN treatment) are all expected to result in an increase in the ratio of NADH/NAD$^+$. Our studies suggest that the fluorescence lifetime of both the free and the protein-bound components of NADH and the ratio of free to protein-bound NADH is related to changes in the NADH/NAD$^+$ ratio. (Cancer Res 2005; 65(19): 8766-73)

Introduction

In the presence of oxygen, eukaryotic cells depend on the mitochondrial electron-transport chain to produce useful chemical energy in the form of ATP. The first complex of this system, NAD$^+$ (an active coenzyme of niacin), functions as an important intermediary in the transfer of two electrons for cellular energy metabolism. Although it exists in an oxidized (NAD$^+$) and a reduced (dihydro-NAD$^+$, NADH) form, the photo-physics is such that NADH is an intrinsically fluorescent molecule, whereas its oxidized product (NAD$^+$) is not. In 1962, Chance et al. exploited this phenomenon to show that microfluorometry of NADH in intact cells and tissues gives a continuous measurement of intracellular oxidation-reduction states *in vivo* (1). This pioneering work served as a precursor for a variety of studies that used direct monitoring of NADH fluorescence to dynamically interpret the metabolic activity within the cell (2, 3). An intuitive application of this technique is to study carcinogenesis in a variety of organ sites such as the breast, which are known to have increased metabolic rates (4). In the past decade, several groups have shown using quantitative NADH fluorescence measurements from tissues in a variety of different organs (including the breast and oral cavity) that significant differences exist between malignant and normal tissue types (5–8).

Recently, there has been considerable attention given to spectrally and time-resolved studies of NADH fluorescence (9–12). A key advantage of the time resolved method is that the excited-state lifetime of a fluorophore is independent of its concentration. Furthermore, because the lifetime of the fluorophore directly relates to its microenvironment, this method can obtain information about the interaction of the fluorophore with the surrounding system (13). Because the fluorescence lifetime of intracellular NADH molecules that coexist in both bound (localized mainly within the mitochondria) and free (localized mainly within the cytoplasm) forms are inherently different (14), this technique can be used to quantify the ratio of the free and bound forms of NADH despite the fact that both have similar spectral characteristics (15).

The first fluorescence lifetime imaging (FLIM) studies of the free and bound forms of NADH was reported by Lakowicz et al. in 1992, where lifetime values of unbound NADH (free in solution) and NADH bound to malate dehydrogenase were obtained to reveal distinct differences in the excited-state lifetimes of the two species (16). This critical investigation suggested that FLIM-based techniques have the potential to provide researchers with functional maps of free and protein-bound forms of NADH and their corresponding lifetimes. FLIM of free and protein-bound NADH in cultivated endothelial cells from calf aorta (17) revealed lifetime values of ~0.4 to 0.5 and 2.0 to 2.5 nanoseconds for free and bound molecules, respectively. A few studies have been reported that exploit the intrinsic fluorescence lifetime of NADH for discriminating between malignant and nonmalignant cells/tissues. Time-resolved fluorescence studies of metastatic and nonmetastatic murine melanoma cell lines, as well as human tumorigenic lung cancer and bronchiolar epithelial cells, showed that the average lifetime of NADH was lower in metastatic cells than in nonmetastatic cells (9). Specifically, nonmalignant cells exhibited mean lifetimes in the range of 1.4 to 1.9 nanoseconds, whereas malignant cell lifetimes were in the range of 0.5 to 0.85 nanosecond. A single study has been conducted that uses the unique properties of FLIM to study breast cancer, primarily to show the feasibility of this approach for histopathologic assessment (18). This study, which used fixed but unstained tissue sections revealed statistically significant differences in the fluorescence lifetimes of benign and malignant tissues. Whereas this was the first FLIM study to be conducted that directly compared benign versus malignant breast tissue, the effects of

Requests for reprints: Kevin W. Eliceiri, University of Wisconsin-Madison, Room 271, Animal Sciences, 1675 Observatory Drive, Madison, WI 53706. Phone: 608-263-6288; Fax: 608-262-4570; E-mail: eliceiri@wisc.edu.

doi:10.1158/0008-5472.CAN-04-3922

sample fixation are likely to significantly alter fluorescence lifetimes compared with that of unfixed tissue. When recording the fluorescence lifetimes of metabolites related to cellular metabolism, it is clearly preferable to use viable cells and tissues.

In this article, we present a novel method for deriving functional maps of intracellular reduction-oxidation states ($NADH/NAD^+$ ratio) *in vivo* via measurement of the fluorescence lifetimes and the ratio of free to protein-bound NADH using two-photon FLIM. We measured the fluorescence decay curve of human breast cells at a two-photon excitation wavelength of 740 nm, which was resolved into short and long lifetime components with similar lifetimes to those described in the literature for the free and protein-bound forms of NADH, respectively. We show the feasibility of this technique for measuring changes in $NADH/NAD^+$ ratio by dynamically imaging the normal MCF10A human breast cell line with subcellular resolution at an early, logarithmic, and confluent phase of the cellular growth curve and then under a variety of perturbations including serum starvation and inhibition of electron transport using potassium cyanide (KCN).

Materials and Methods

Sample Preparation, Experiments, and Viability Assessment

MCF10A cells were obtained from the American Type Culture Collection.[4] The cells remained free of *Mycoplasma* and other contaminants and were propagated by adherent culture according to established protocols (19). MCF10A cells used in this study were transfected with an "empty" vector, pZIP. For control experiments, MCF10A-pZIP cells were grown in DMEM-F12 supplemented with 5% horse serum, 20 ng/mL epidermal growth factor, 10 μg/mL insulin, and 0.5 μg/mL hydrocortisone. Plated cells were stored in a 10% CO_2 incubator at 37°C and cultured every 3 to 4 days. Cells were detached from the flasks by trypsinization and triply washed in 10 mL of PBS. A hemacytometer was used to determine the concentration of the cells by counting the number of cells per milliliter. An independent count was taken from each grid on the hemacytometer to obtain an SD for the cell concentration. Upon determination of the concentration of the cells, the volumes required to plate 25,000, 100,000, and 1,000,000 cells were calculated, respectively. These concentrations were chosen to result in confluences that approximated an early, mid (logarithmic), and late (confluent) point on the cellular growth curve. MCF10A-pZIP cells at the three different confluences were plated on lysine-coated cover glass bottom Petri dishes (size, 35 mm; P35G-0-41-C, MatTek, Ashland, MA) and immersed in their standard growth media. Six independent imaging sessions were conducted over the course of ~1 month. For any given session, three independent dishes at the three different cell confluences (25,000, 100,000, and 1,000,000 cells) were plated the day before and permitted to grow overnight in the incubator. Thus, a total of 18 (6 × 3) individual samples were imaged with multiphoton FLIM to complete the control study.

Perturbation study: serum starvation. To deprive the cells of growth factors, the growth of the MCF10A-pZIP cells was disturbed through serum starvation. Three independent imaging sessions were conducted. For any given session, three independent dishes at the three different cell confluences (25,000, 100,000, and 1,000,000 cells) were plated, except that instead of allowing the cells to grow overnight in their standard growth medium, the normal growth medium was removed and replaced with medium containing no serum for a period of 14 hours. A total of nine (3 × 3) individual samples were imaged with multiphoton FLIM to complete the serum starvation study.

Perturbation study: KCN treatment. To inhibit electron transport, KCN was added to the MCF10A-pZIP cells. Three independent imaging sessions were carried out. For any given session, three independent dishes at the three different confluences (25,000, 100,000, and 1,000,000 cells) were plated the day before and permitted to grow overnight in the incubator. During each imaging session, the cells were imaged before and immediately after 1 mL of 4 mmol/L KCN (Sigma Chemical Co., St. Louis, MO) was added to the standard growth media. The administration of KCN was carefully monitored to ensure that the attached cells were not disturbed within the microscopic field of view. Ten images were acquired after addition of KCN in ~75-second intervals, 60 seconds of which was the photon-counting process. It should be pointed out that a different microscopic field of view was imaged at each interval to eliminate the effects of photobleaching. A total of nine (3 × 3) individual samples were imaged with multiphoton FLIM to complete the KCN treatment study.

Viability assessment. At the completion of the final image acquisition, cell viability was confirmed under light microscopy (using the same microscope) by trypan blue exclusion, which was done without moving the sample and observing the same field as that imaged with multiphoton FLIM. All three confluences were imaged under identical experimental conditions and remained viable throughout any given imaging session.

Instrumentation

A detailed description of the multiphoton FLIM has been given elsewhere (20). Briefly, the system consists of a Ti:Sapphire mode-locking laser cavity (Coherent Mira, Coherent, Santa Clara, CA) pumped by an 8-W solid-state laser (Coherent Verdi), an inverted microscope (Diaphot 200, Nikon, Melville, NY), a confocal scanning unit (MRC-600, Bio-Rad, Hercules, CA), and a fast photon-counting detector (PMH-100, Becker & Hickl GmbH, Berlin, Germany). The laser beam is coupled to the confocal scanning unit and inverted microscope to produce a focused scanning spot that moves across the normal focal plane of an imaging objective. Upon exiting the scanning unit, the laser beam is passed to the microscope through a transfer lens (01LAO159, Melles Griot, Rochester, NY) and impinges on a dichromatic mirror (650DCSP, Chroma, Inc., Rockingham, VT) mounted at 45 degrees in the sliding filter block of the microscope. This mirror efficiently directs incident illumination up to fill the back aperture of an imaging objective (60× 1.4 NA, oil, Nikon) while permitting the emitted visible fluorescent light from the sample to be transmitted to a fast photon-counting detector (PMH-100, Becker & Hickl). Multiphoton FLIM images are acquired with a complete electronic system for recording fast light signals by time-correlated single photon counting (SPC-830, Becker & Hickl). Synchronized fluorescence lifetime data collection on a pixel-by-pixel basis is achieved using the x and y laser scanning signals generated for the confocal scan unit.

Imaging Variables

NADH has an absorption spectrum that peaks at a wavelength of 350 nm and emits a fluorescence spectrum with a peak wavelength of ~450 nm (16). For multiphoton FLIM, the laser was tuned to the temporally stable wavelength of 740 nm, which is close to the ideal two-photon absorption peak of NADH. For cellular imaging, the mean power was adjusted to ~3.3 to 3.7 mW at the sample to obtain a sufficient photon count rate. Beginning with the lowest confluence (25,000), images were obtained on the multiphoton microscope. Five separate images of grouped cells were collected per dish, with the *minimum* spacing between observed groups being ~200 μm. Therefore, the total number of images acquired in the control and serum starvation experiments was the product of the number of images per dish ($n = 5$), the number of confluences ($n = 3$), and the number of imaging sessions [i.e., $n = 90$ ($5 \times 3 \times 6$) and $n = 45$ ($5 \times 3 \times 3$), respectively]. The total number images acquired in the KCN treatment experiment was 45 ($5 \times 3 \times 3$) before treatment (this is already included as part of the control cell study data). The total number of images acquired after KCN treatment was the product of the number of images per dish (one image per dish was taken at five different time intervals), the number of confluences ($n = 3$), and the number of imaging sessions [$n = 3$; i.e., $n = 45$ ($5 \times 3 \times 3$)]. Single-photon counting was done at a rate of ~500×10^5 photons/s for 60 seconds with an average pixel dwell time of ~6.5 microseconds.

Imaging Standards

To ensure accuracy of all fluorescence lifetimes measured in the experiments, the lifetime of a known and stable instrument standard

[4] http://www.atcc.org

(YG Microspheres, 20 μm diameter, Polysciences, Inc., Warrington, PA) was measured before all cellular imaging. This was achieved by locating ~5 to 10 microspheres and imaging at an illumination power of ~1.5 mW at the sample. This level of power was selected to yield a photon count rate comparable with that used in our cellular imaging protocol, whereas the collection variables remained unchanged. At the completion of the cellular imaging experiments, the instrument standard was reimaged to ensure no changes to the instrument had occurred during the experiment (i.e., lifetime or intensity). The measured lifetime was ~2.2 ± 0.1 nanoseconds (averaged from all experimental days), which is consistent with that reported in literature.

The instrument response function (IRF) of the optical system was measured using second harmonic generated signal from a β-BaB_2O_4 crystal (20). The measured full width at half maximum of the IRF was determined to be ~190 ± 2 picoseconds. It should be pointed out that this represents the IRF of the *overall* system where the components that mainly contribute to temporal degradation are the transient time spread of the detector, optical dispersion at mirrors and through lenses, and light scattering at diaphragms.

Analytic Methods

The fluorescence intensity of single cells was investigated using offline software (SPCImage, Becker & Hickl) by summing individual photon counts over all time channels for each pixel. For the analysis of fluorescence lifetimes obtained in this study, the same software was used, which is capable of modeling up to a three-exponential fluorescence decay distribution. The program uses a deconvolution technique in conjunction with the measured instrument response function to yield a fluorescence decay curve that is corrected for the instrument response. A Levenberg-Marquardt routine for nonlinear fitting (21) was used to fit the deconvolved fluorescence decay curve to a model function of the form:

$$I(t) = \sum_{i=0}^{n} a_i \exp^{(-t/\tau_i)} + c \qquad \text{(A)}$$

where $I(t)$ is the fluorescence intensity at time t after the excitation pulse, n is the total number of decaying species in the exponential sum, and c is a constant pertaining to the level of background light present in most practical situations. The variables τ_i and a_i are the fluorescence lifetime and fractional contribution of the ith emitting species, respectively. The free variables in this model were c, τ_i, and a_i. A time-optimized procedure was used to determine a statistical measure of the quality of the fit via the minimum reduced (weighed; ref. 2). The quality of the nonlinear curve fit for any given pixel (and hence that of the entire reconstructed image) depends, to a large extent, on the IRF of the system, because it is convolved with the time slope of the (multi) exponential decay (22). Theoretically, this value is 1.0 for an ideal fit; however, in practice, values may be larger due to disturbances of the IRF and other systematic errors, the most problematic being the detector dark count and background noise.

A systematic analysis of fluorescence decay curves with the FLIM system was conducted in the following manner. For any given imaging session (i.e., day), the best four images (those with the highest signal to noise ratio) of the five images acquired for each confluence (25,000, 100,000, or 1,000,000 cells) were selected and analyzed. A two-exponential decay model was applied to individually fit four representative pixels (see Discussion for an alternative approach) from each of these samples with a binning factor (n) of 1. This factor defines how many adjacent pixels are combined before the decay time is calculated according to the relation $(2n + 1)^2$ (2). Therefore, for a binning factor of 1, the fluorescence decay curve for each pixel analyzed was summed over nine immediately adjacent pixels. It should be pointed out that although this technique results in a decrease in spatial resolution, the accuracy of the fluorescence lifetime decay time is significantly increased (23). At each representative pixel, the short and the long fluorescence lifetime components were extracted along with their relative contributions. The average values and SD of each of these variables per dish were determined from the total number of representative pixels analyzed for a given confluence (i.e., four pixels per image) multiplied by the number of images per dish (n = 4 for the control and serum starvation experiments and n = 5 for the post-KCN treatment experiments).

Results

Figure 1 shows two consecutively recorded multiphoton fluorescence intensity images of MCF10A Pzip cells at a 1,000,000 confluence. All images were obtained under identical experimental conditions at 740-nm excitation and the intensities are shown in gray scale over the same range. The first image (*left*) was collected over a period of 60 seconds and the second image (*right*) was collected over a period of 60 seconds immediately after the first image was recorded. It can be seen that the two images have very similar intensities and intensity distribution, indicating that the MCF10A pZIP cells were not photobleached under the imaging conditions used. To further minimize the effects of photobleaching, no microscopic field of view was imaged more than once in this study.

Figure 2 shows a fluorescence lifetime decay curve (blue), the instrument response function (green), best fit (red), and residuals (black) of a single pixel selected from within a multiphoton fluorescence intensity image of an MCF10A pZIP cell in a monolayer of cells at a 1,000,000 confluence. It can be seen that the quality of the fit to the lifetime decay curve is excellent as

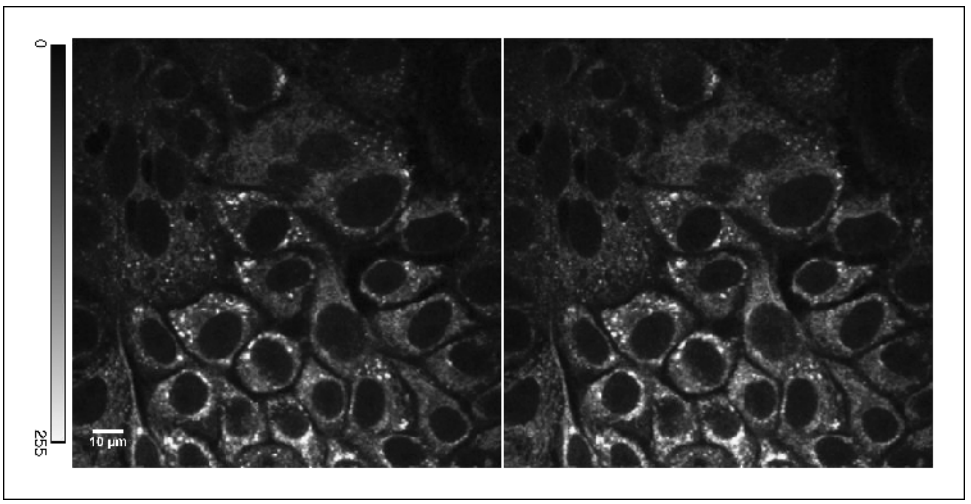

Figure 1. Two consecutively recorded multiphoton fluorescence intensity images of MCF10A Pzip cells at a 1,000,000 confluence. All images were obtained under identical experimental conditions at 740-nm excitation and the intensities are shown in gray scale over the same range. The first image (*left*) was collected over a period of 60 seconds and the second image (*right*) was collected over a period of 60 seconds immediately after the first image was recorded.

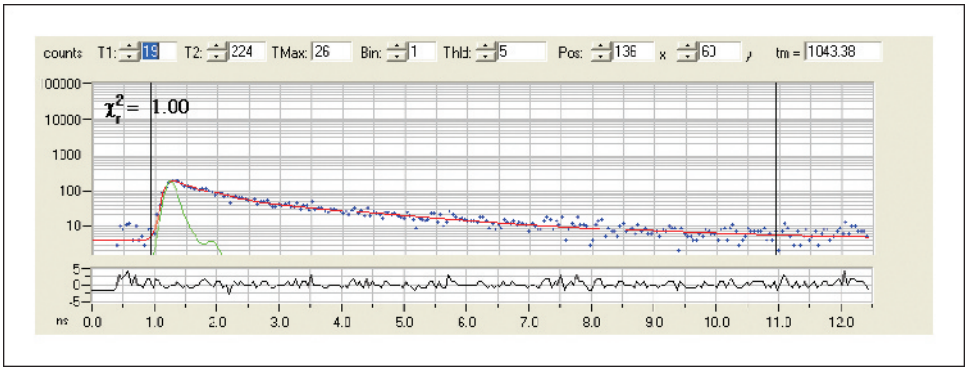

Figure 2. Fluorescence lifetime decay curve (*blue*), the instrument response function (*green*), best fit (*red*), and residuals (*black*) of a single pixel selected from within a multiphoton fluorescence intensity image of an MCF10A pZIP cell in a monolayer of cells at a 1,000,000 confluence. It can be seen that the quality of the fit to the lifetime decay curve is excellent as evidenced by the residual and the χ^2 value of 1 (*y*-axis is in photon counts and *x*-axis is time in nanoseconds).

evidenced by the residual and the χ^2 value of 1. This is representative of all fits obtained in this study.

Effect of cell confluence on the lifetimes and ratio of free and protein-bound NADH. Figure 3 shows representative fluorescence lifetime images of MCF10A pZIP cells at (a) an early (25,000 cells), (b) mid (100,000 cells; logarithmic), and (c) late (1,000,000 cells; confluent) point on the cellular growth curve. The pseudocolor mapping has been chosen to represent that of the average of the short (τ_1) and the (τ_2) lifetime components weighed by their relative contributions, a_1 and a_2, respectively [i.e., $\tau_m = (a_1\tau_1 + a_2\tau_2) / (a_1 + a_2)$]. All images were obtained under identical experimental conditions at 740-nm excitation and are pseudocolor mapped over the same range. It is clearly shown in Fig. 3*A-C* that cells of a higher confluence exhibit a decrease in τ_m, mainly due to the fact that the contribution of and absolute value of τ_2 significantly decreases with increasing confluence.

Table 1 shows the fluorescence lifetimes of free (τ_1) and protein-bound NADH (τ_2) and their and the ratio of their relative contribution (a_1:a_2) at the three different cell confluences (25,000, 100,000, and 1,000,000) for $n = 6$ experimental control days with the averages and SD for any given imaging session (16 data points) and the combined average and SD for all imaging sessions (96 data points). It can be seen that there is excellent consistency in the fluorescence lifetimes and free to protein-bound ratio of NADH between the six independent imaging sessions. The measured lifetimes for free and protein-bound NADH correlate well with those reported by several other groups (17, 24, 25) which are in the range of ~0.3 to 0.5 and 2.0 to 3.2 nanoseconds, respectively.

Figure 4 shows the average and SDs (for all six imaging sessions combined in Table 1) of the fluorescence lifetimes and ratios of free and protein-bound NADH as a function of cell confluence. It is clear that any given phase of the growth cycle can be clearly discerned via multiple variables of the fluorescence exponential decay. First, the average fluorescence lifetime of protein-bound NADH is reduced by a factor of ~2 from 25,000 to 1,000,000 confluence. The average fluorescence lifetime of free NADH is also reduced as the cell confluence increases from 25,000 to 1,000,000. Additionally, the ratio of free and protein-bound NADH (a_1:a_2) increases by more than a factor of 2 from the early to confluent phase of the growth curve. A one-way ANOVA test showed statistically significant differences ($P < 0.01$) in the lifetimes and ratio of the free and protein-bound NADH with increasing confluence.

Perturbation study: serum starvation. Figure 5 shows the average and SDs (for all three imaging sessions combined) of the fluorescence lifetimes and ratios of free and protein-bound NADH as a function of confluence for cells that have been serum starved. A comparison was made between the data shown in Figs. 4 and 5 using a Student's *t* test. The average lifetime of protein-bound NADH was found to be statistically lower than that of control cells at all three confluences ($P > 0.05$). The average lifetime of free NADH for confluences of 25,000 and 100,000 were also statistically lower than that of control cells ($P < 0.05$). However, the average lifetime of free NADH at a 1,000,000 confluence shows no statistically significant difference compared with that of the control cells. The ratio of free and protein-bound NADH in the serum-starved cells was statistically higher than that of the control cells at all three confluences ($P < 0.05$).

Perturbation study: KCN treatment. Table 2 shows the fluorescence lifetimes of free (τ_1) and protein-bound NADH (τ_2) and the ratio of their relative contribution (a_1:a_2) at the three different cell confluences (25,000, 100,000, and 1,000,000) for 1, 3, 5, 7, and 10 minutes after addition of 1 mL of 4 mmol/L KCN with the averages and SD for all three imaging sessions combined (12 data points) and the combined average and SD for all time points and imaging sessions (60 data points). Table 2 revealed statistically insignificant differences between the measured values at the different time intervals post addition of KCN. Thus, the fluorescence

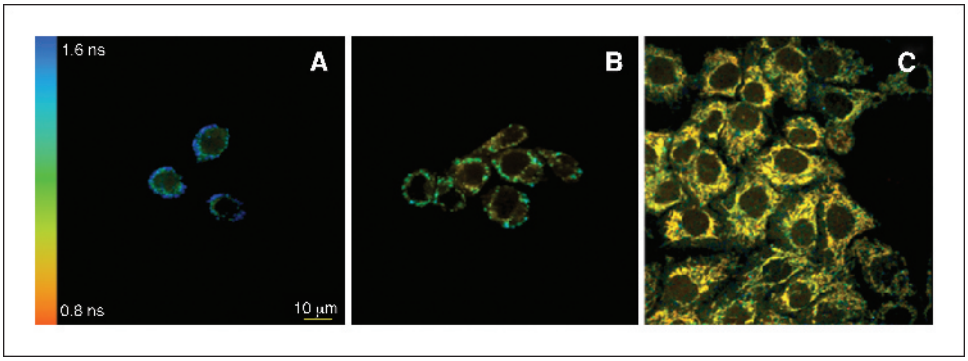

Figure 3. Representative fluorescence lifetime images of MCF10A pZIP cells at (*A*) an early (25,000 cells), (*B*) mid (100,000 cells, logarithmic), and (*C*) late (1,000,000 cells, confluent) point on the cellular growth curve. The pseudocolor mapping has been chosen to represent that of the average of the short (τ_1) and the (τ_2) lifetime components weighted by their relative contributions, a_1 and a_2, respectively [i.e., $\tau_m = (a_1\tau_1 + a_2\tau_2) / (a_1 + a_2)$]. All images were obtained under identical experimental conditions at 740-nm excitation and are pseudocolor mapped over the same range.

Table 1. Fluorescence lifetimes of free (τ_1) and protein-bound NADH (τ_2) and the ratio of their relative contribution (a_1:a_2) at the three different cell confluences (25,000, 100,000, and 1,000,000) for n = 6 experimental control days with the averages and SD for any given imaging session (16 data points) and the combined average and SD for all imaging sessions (96 data points)

Confluence	25,000			100,000			1,000,000		
	τ_1 (ns) ± 0.05	τ_2 (ns) ± 0.1	Ratio (a_1:a_2)	τ_1 (ns) ± 0.05	τ_2 (ns) ± 0.1	Ratio (a_1:a_2)	τ_1 (ns) ± 0.05	τ_2 (ns) ± 0.1	Ratio (a_1:a_2)
n = 1	0.427	3.137	1.223	0.366	2.548	1.917	0.353	1.725	2.750
n = 2	0.388	2.920	1.015	0.393	2.588	1.743	0.355	1.735	2.900
n = 3	0.428	3.209	0.998	0.420	2.674	1.797	0.350	1.753	2.929
n = 4	0.455	3.190	1.167	0.420	2.586	2.051	0.346	1.720	2.875
n = 5	0.404	3.114	1.350	0.398	2.559	1.844	0.339	1.708	2.300
n = 6	0.433	3.067	1.298	0.388	2.434	1.972	0.358	1.700	2.458
Average	0.423	*3.106*	1.175	0.398	2.565	1.888	0.350	1.723	2.702
SD	0.023	0.105	0.145	0.021	0.078	0.115	0.007	0.019	0.262

lifetimes and the ratio of free and protein-bound NADH were averaged over the five time intervals to facilitate comparison between KCN-treated and control cells as well as between KCN-treated cells at different confluences as shown in Fig. 6.

Figure 6 shows the average and SDs (for all three imaging sessions combined) of the fluorescence lifetimes and ratios of free and protein-bound NADH as a function of confluence for MCF10A pZIP cells that have been treated with KCN. The lifetimes and ratios have been averaged for all time points (1, 3, 5, 7, and 10 minutes) after the KCN administration. The addition of KCN yields results that are very similar to that of the serum starvation experiments (see Fig. 5). The only difference is that the average lifetime of protein-bound NADH is not statistically different from that of controls cells at a 1,000,000 confluence (see Fig. 4). The total number of photons detected in a single pixel before and after the addition of KCN was compared, which showed that the fluorescence intensity increased by a factor of ~1.3 after addition of KCN, which is consistent with observations reported in independent studies (25–27).

Discussion

There are a number of factors that support our underlying hypothesis that the fluorescence measured in this study originates from the coenzyme NADH. In breast epithelial cells (MCF10A pZIP), there are three principle fluorophores: NADH, flavin adenine dinucleotide (FAD), and tryptophan, the spectral characteristics of which have been characterized previously (28). At the equivalent single-photon excitation wavelength used in this study (370 nm), the fluorescence spectrum measured from the MCF10A pZIP cells has the same spectrum as NADH (28). Second, it is well known that the addition of KCN to cells will inhibit electron transport and thus the ratio of NADH and NAD^+ (29). This will cause an increase in the fluorescence intensity of NADH. In the KCN study reported in this article, the fluorescence intensity increased by a factor of ~1.3 after addition of KCN, which is consistent with what is expected (25–27). Finally, the average fluorescence lifetimes recorded for the two fluorescence emitting species in the MCF10A pZIP cells in this study are consistent with that reported for free and bound NADH

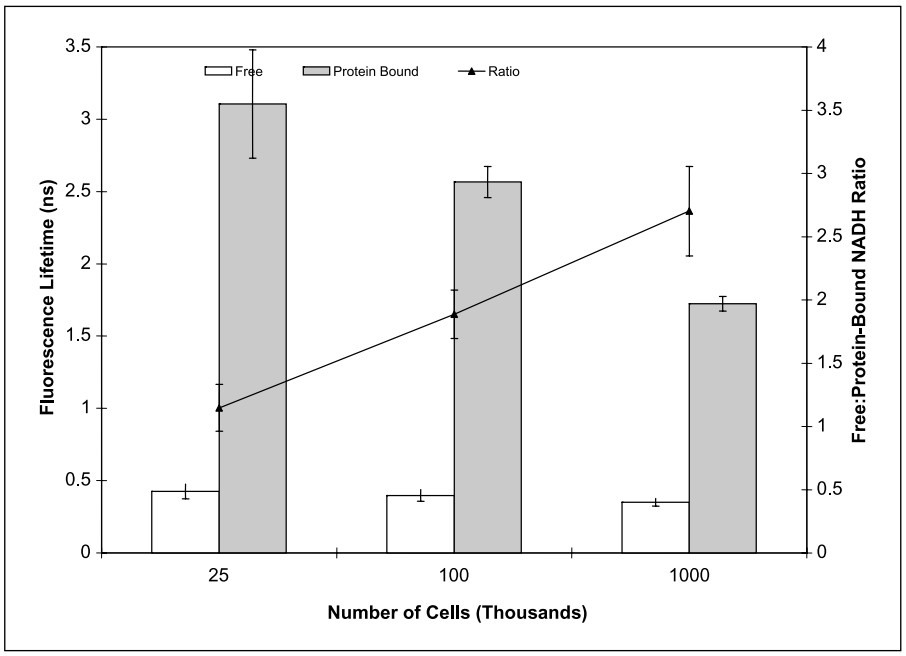

Figure 4. Average and SDs (for all six imaging sessions combined) of the fluorescence lifetimes and ratios of free and protein-bound NADH as a function of cell confluence.

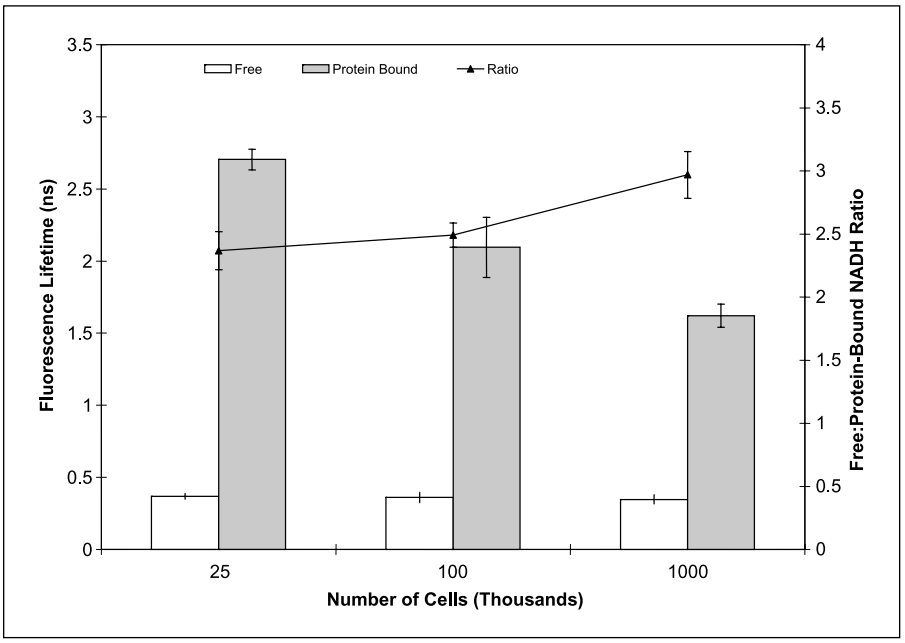

Figure 5. Average and SDs (for all three imaging sessions combined) of the fluorescence lifetimes and ratios of free and protein-bound NADH as a function of confluence for cells that have been serum starved.

in the literature (17, 24, 25). It is unlikely that tryptophan will contribute to the fluorescence at a two-photon excitation wavelength of 740 nm, because it has a single-photon absorption peak of ~280 nm (30). Efficient two-photon excitation of tryptophan can be achieved at a wavelength of ~560 nm (30), which is far from the 740-nm excitation used in our experiments. This, combined with the fact that compared with NADH and FAD, tryptophan has a particularly low two-photon absorption cross-section (31), would deem it an improbable source of the fluorescence measured in this study. It should also be pointed out that the measured fluorescence lifetimes in Results (Effect of cell confluence on the lifetimes and ratio of free and protein-bound NADH) are shorter in all cases by a factor of ~2 compared with that reported for FAD (24).

An increase in cell confluence increases cell crowding and thus likely decreases oxygen consumption. A decrease in oxygen consumption should in turn increase the NADH/NAD^+ ratio. It can be inferred from the results of the control study that a decrease in the fluorescence lifetime of both the free and protein-bound components of NADH and a decrease in the contribution of protein-bound NADH with increasing confluence is related to an increase in the NADH/NAD^+ ratio.

KCN treatment inhibits electron transport (29). This should also result in an increase in the NADH/NAD^+ ratio. Thus, it can be inferred that the decrease in the fluorescence lifetime of the free and protein-bound components of NADH of KCN-treated cells at confluences of 25,000 and 100,000 and a decrease in the contribution of protein-bound NADH of KCN-treated cells at all three confluences is related to an increased NADH/NAD^+ ratio. This corroborates the experimental findings from the control study. However, the lack of statistically significant differences between the fluorescence lifetime of protein-bound and free NADH in the KCN-treated and control cells at a confluence of 1,000,000 is not clear at this time. It is speculated that KCN treatment does not further affect the NADH/NAD^+ ratio of the fully confluent cells.

Serum is full of precursors for both glycolysis (such as glucose) and the citric acid cycle (such as pyruvate), which under normal

Table 2. Fluorescence lifetimes of free (τ_1) and protein-bound NADH (τ_2) and the ratio of their relative contribution (a_1:a_2) at the three different cell confluences (25,000, 100,000, and 1,000,000) for 1, 3, 5, 7, and 10 minutes after addition of 1 mL of 4 mmol/L KCN with the averages and SD for all three imaging sessions combined (12 data points) and the combined average and SD for all time points and imaging sessions (60 data points)

Confluence	25,000			100,000			1,000,000		
Time lapsed (min)	τ_1(ns) ± 0.05	τ_2(ns) ± 0.1	Ratio (a_1:a_2)	τ_1 (ns) ± 0.05	τ_2 (ns) ± 0.1	Ratio (a_1:a_2)	τ_1 (ns) ± 0.05	τ_2 (ns) ± 0.1	Ratio (a_1:a_2)
1	0.423	2.05	2.1	0.381	1.72	2.34	0.503	2.05	3.41
3	0.391	1.93	2.0	0.401	1.91	2.41	0.461	1.91	3.55
5	0.411	2.15	2.2	0.352	1.75	2.28	0.422	1.82	3.72
7	0.382	1.95	2.2	0.361	1.82	2.33	0.491	1.96	3.42
10	0.385	2.07	2.0	0.373	1.73	2.31	0.473	1.88	3.82
Average	0.397	2.024	2.101	0.372	1.770	2.334	0.468	1.922	3.574
SD	0.017	0.099	0.097	0.019	0.084	0.098	0.031	0.087	0.174

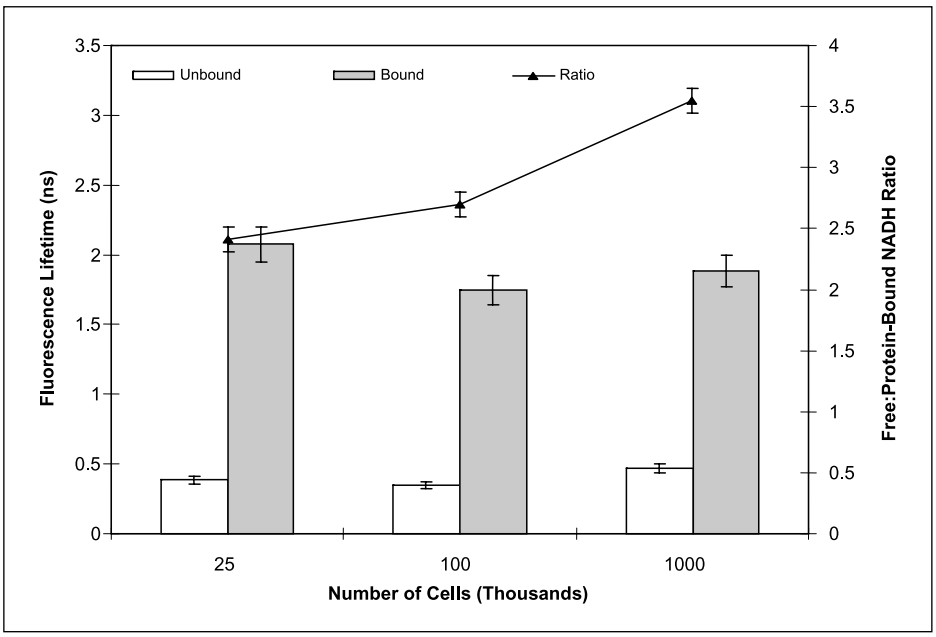

Figure 6. Average and SDs (for all three imaging sessions combined) of the fluorescence lifetimes and ratios of free and protein-bound NADH as a function of confluence for cells that have been treated with KCN. The lifetimes and ratios have been averaged for all time points (1, 3, 5, 7, and 10 minutes) after the KCN administration.

conditions are essential for cellular metabolism (29). Therefore, removal of serum is expected to slow down cellular metabolism and shift the reduction-oxidation ratio towards increased NADH. Thus, it is not surprising that serum-starved and KCN-treated cells yield similar changes in the fluorescence lifetimes and relative contributions of free and protein-bound NADH relative to that of control cells.

Previous studies of NADH in cell culture found that the effective lifetime of NADH (mean lifetime of free and protein-bound NADH) decreases with oxidative stress induced with the respiratory chain inhibitor rotenone (17). KCN, like rotenone, is a respiratory chain inhibitor and has a similar effect on the lifetime of free and protein-bound NADH in our study. In another study, multiphoton microscopy of lifetime and anisotropy in brain tissue slices revealed lifetime shortening with hypoxia and this was attributed to a redistribution of protein-bound NADH to enzyme binding sites with shorter lifetimes and due to a decrease in the lifetime of free NADH (32). KCN treatment, like hypoxia, caused a decrease in the lifetime of both protein-bound and free NADH in our study. Both KCN and hypoxia cause an increase in the NADH/NAD^+ ratio (KCN inhibits the transfer of electrons from NADH to oxygen and hypoxia reduces the supply of oxygen that can accept electrons from NADH). Thus, the lifetime shortening caused by both hypoxia and KCN is likely related to an increased ratio of NADH/NAD^+.

In addition to lifetime imaging, cell proliferation was determined using propidium iodide staining and flow cytometry in the serum starved and control cells at the three different confluences. Results averaged from a total of two independent experiments showed that there is negligible difference in the percentage of cells in S-G_2-M phase for the control or serum starved cells at different confluences. However, a parallel imaging experiment done on cells plated on the same day and under the same conditions showed a decrease in the fluorescence lifetime of free and protein-bound NADH and a decrease in the contribution of protein-bound NADH with increased plating density and serum starvation (consistent with Figs. 4 and 5). This additional study indicates that the observed changes in the fluorescence lifetime variables are not due to changes in cell proliferation.

In the current study, lifetime analyses were done on several pixels per cell (which were arbitrarily identified from the cytoplasmic region). To test the robustness of this approach, lifetime analyses were also done on all pixels from the cytoplasmic region of the cell. Both methods of analysis yielded very similar results (this was only evaluated on images collected from control cells at different confluences) thus indicating that the method of analysis does not affect the conclusions reported in this study.

Conclusion

This article describes changes in the fluorescence lifetimes and contributions of fluorescence emitting species in normal human breast epithelial cells at a two-photon excitation wavelength of 740 nm that correlate well with imposed changes in the intracellular reduction-oxidation ratio. Based on previous studies, we infer that these fluorescence signals likely arise from the protein-bound and free forms of NADH. Our studies suggest that the fluorescence lifetime of both the free and the protein-bound components of NADH and the ratio of free to protein-bound NADH is related to changes in the NADH/NAD^+ ratio.

The key advantage of using the lifetime components rather than the intensity of NADH is that the lifetime is independent of NADH concentration and does not need to be calibrated for variations in the throughput of the instrument. We expect the outcome of this study to be a precursor for future work directed at functional mapping of normal and malignant breast epithelial cells, which may provide a novel way to track carcinogenesis in breast cells and ultimately, in breast tissues.

Acknowledgments

Received 11/2/2004; revised 5/30/2005; accepted 7/26/2005.

Grant support: NIH NIBIB grant R01-EB000184.

The costs of publication of this article were defrayed in part by the payment of page charges. This article must therefore be hereby marked *advertisement* in accordance with 18 U.S.C. Section 1734 solely to indicate this fact.

We thank A. Ada-Nguema, G. Palmer, and M. Skala for assistance and discussions.

References

1. Chance B, Cohen P, Jobsis F, Schoener B. Intracellular oxidation-reduction states *in vivo*. Science 1962;137:499–508.
2. Chance B, Williamson JR, Famieson D, Schoener B. Properties and kinetics of reduced pyridine nucleotide fluorescence of the isolated and *in vivo* rat heart. Biochem Z 1965;341:357–77.
3. Pappajohn DJ, Penneys R, Chance B. NADH spectrofluorometry of rat skin. J Appl Physiol 1972;33:684–7.
4. Avril N, Menzel M, Dose J, et al. Glucose metabolism of breast cancer assessed by 18F-FDG PET: histologic and immunohistochemical tissue analysis. J Nucl Med 2001;42:9–16.
5. Gupta PK, Majumder SK, Uppal A. Breast cancer diagnosis using N2 laser excited autofluorescence spectroscopy. Lasers Surg Med 1997;21:417–22.
6. Majumder SK, Gupta PK, Jain B, Uppal A. UV excited autofluorescence spectroscopy of human breast tissues for discriminating cancerous tissue from benign tumor and normal tissue. Lasers Life Sci 1999;8:249–64.
7. Schomacker KT, Frisoli JK, Compton CC, et al. Ultraviolet laser-induced fluorescence of colonic tissue: basic biology and diagnostic potential. Lasers Surg Med 1992;12:63–78.
8. Ramanujam N, Mitchell MF, Mahadevan A, et al. *In vivo* diagnosis of cervical intraepithelial neoplasia using 337-nm-excited laser-induced fluorescence. Proc Natl Acad Sci U S A 1994;91:10193–7.
9. Pradhan A, Pal P, Durocher G, et al. Steady state and time-resolved fluorescence properties of metastatic and non-metastatic malignant cells from different species. J Photochem Photobiol B 1995;31:101–12.
10. Pogue BW, Pitts JD, Mycek MA, et al. *In vivo* NADH fluorescence monitoring as an assay for cellular damage in photodynamic therapy. Photochem Photobiol 2001;74:817–24.
11. Konig K, Berns MW, Tromberg BJ. Time-resolved and steady-state fluorescence measurements of β-nicotinamide adenine dinucleotide-alcohol dehydrogenase complex during UVA exposure. J Photochem Photobiol B 1997;37:91–5.
12. Buchner M, Huber R, Sturchler-Pierrat C, Staufenbiel M, Riepe MW. Impaired hypoxic tolerance and altered protein binding of NADH in presymptomatic APP23 transgenic mice. Neuroscience 2002;114:285–9.
13. Wang XF, Periasamy A, Herman B. Fluorescence lifetime imaging microscopy (FLIM): instrumentation and applications. Crit Rev Annal Chem 1992;23:365–9.
14. Wakita M, Nishimura G, Tamura M. Some characteristics of the fluorescence lifetime of reduced pyridine nucleotides in isolated mitochondria, isolated hepatocytes, and perfused rat liver *in situ*. J Biochem (Tokyo) 1995;118:1151–60.
15. Ladokhin AS, Brand L. Evidence for an excited-state reaction contributing to NADH fluorescence. J Fluor 1995;5:99–106.
16. Lakowicz JR, Szmacinski H, Nowaczyk K, Johnson ML. Fluorescence lifetime imaging of free and protein-bound NADH. Proc Natl Acad Sci U S A 1992;89:1271–5.
17. Schneckenburger H, Wagner M, Weber P, Strauss WS, Sailer R. Autofluorescence lifetime imaging of cultivated cells using a UV picosecond laser diode. J Fluor 2004;14:649–54.
18. Tadrous PJ, Siegel J, French PM, Shousha S, Lalani el N, Stamp GW. Fluorescence lifetime imaging of unstained tissues: early results in human breast cancer. J Pathol 2003;199:309–17.
19. Keely PJ, Fong AM, Zutter MM, Santoro SA. Alteration of collagen-dependent adhesion, motility, and morphogenesis by the expression of antisense α 2 integrin mRNA in mammary cells. J Cell Sci 1995;108:595–607.
20. Bird DK, Eliceiri KW, Fan CH, White JG. Simultaneous two-photon spectral and lifetime fluorescence microscopy. Appl Opt 2004;43:5173–82.
21. Press WH, Flannery BP, Teukolsky SA, Vetterling WT. Numerical recipes in C. 2nd ed. Cambridge: Cambridge University Press; 1993.
22. Becker W, Bergmann A, Biskup C, Zimmer T, Klöcker N, Benndorf K. Multi-wavelength TCSPC lifetime imaging. In: San Jose (CA): Biomedical Optics; 2002.
23. Bergmann A. SPCImage: data analysis software for fluorescence lifetime imaging microscopy. 1.6 ed. Berlin: Becker & Hickl GmbH; 2003.
24. Konig K, Riemann I. High-resolution multiphoton tomography of human skin with subcellular spatial resolution and picosecond time resolution. J Biomed Opt 2003;8:432–9.
25. Schneckenburger H, Gschwend MH, Strauss WS, et al. Energy transfer spectroscopy for measuring mitochondrial metabolism in living cells. Photochem Photobiol 1997;66:34–41.
26. Gschwend MH, Rudel R, Strauss WS, Sailer R, Brinkmeier H, Schneckenburger H. Optical detection of mitochondrial NADH content in intact human myotubes. Cell Mol Biol (Noisy-le-grand) 2001;47 Online Pub:OL95–104.
27. Huang S, Heikal AA, Webb WW. Two-photon fluorescence spectroscopy and microscopy of NAD(P)H and flavoprotein. Biophys J 2002;82:2811–25.
28. Palmer GM, Keely PJ, Breslin TM, Ramanujam N. Autofluorescence spectroscopy of normal and malignant human breast cell lines. Photochem Photobiol 2003;78:462–9.
29. Berg JM, Tymoczko JL, Stryer L. Biochemistry 2001. 5th ed. New York: W H. Freeman and Company; 2002.
30. Lippitz M, Erker W, Decker H, van Holde KE, Basche T. Two-photon excitation microscopy of tryptophan-containing proteins. Proc Natl Acad Sci U S A 2002;99:2772–7.
31. Rehms A, Callis P. Two-photon fluorescence excitation spectra of aromatic amino acids. Chem Phys Lett 1993;208:276–82.
32. Vishwasrao HD, Heikal AA, Kasischke KA, Webb WW. Conformational dependence of intracellular NADH on metabolic state revealed by associated fluorescence anisotrophy. J Biol Chem 2005.

Metabolic Mapping of MCF10A Human Breast Cells via Multiphoton Fluorescence Lifetime Imaging of the Coenzyme NADH

Damian K. Bird, Long Yan, Kristin M. Vrotsos, et al.

Cancer Res 2005;65:8766-8773.